

## Article

# Wind Pressure Field Reconstruction and Prediction of Large-Span Roof Structure with Folded-Plate Type Based on Proper Orthogonal Decomposition

Yi Su <sup>1</sup> , Jin Di <sup>1,2,\*</sup>, Jinzhe Li <sup>3</sup> and Fan Xia <sup>1</sup>

<sup>1</sup> Key Laboratory of New Technology for Construction of Cities in Mountain Area, School of Civil Engineering, Chongqing University, Chongqing 400450, China

<sup>2</sup> College of Civil Engineering and Architecture, Zhejiang University, Hangzhou 310058, China

<sup>3</sup> China Southwest Architectural Design and Research Institute Corp., Ltd., Chengdu 610042, China

\* Correspondence: dijin@cqu.edu.cn

**Abstract:** The complex and diverse structural forms make it impossible to define universal shape coefficients for large-span roof structures, which usually need to be obtained by wind tunnel tests. However, the number of test measurement points is limited, which leads to obvious limitations in the study of wind loads on large-span roof structures. Taking a large-span folded-plate roof as an example, based on the wind tunnel pressure test results of the rigid model, the proper orthogonal decomposition (POD) method is used to reconstruct the wind pressure field of the roof using the first several eigenmodes. The wind pressure of several typical characteristic points is predicted based on four different interpolations methods, and the accuracy and feasibility of POD method in reconstruction and prediction of wind pressure field of large-span roof are analyzed and studied from multiple perspectives. The results show that the order of the selected structural eigenmodes has an impact on the reconstruction accuracy of the wind pressure field. The more orders are selected, the closer the wind pressure field reconstruction is to the true value. The reconstruction effect of the wind pressure field based on the POD method is related to the spatial position of the predicted point, and the reconstruction effect of the wind field based on the fluctuating wind pressure is obviously better than the that based on the mean wind pressure. When the POD method is used to predict the wind pressure of an unknown point, different interpolation methods can achieve ideal results. Among them, the bilinear interpolation method has the highest prediction accuracy, and the adjacent point interpolation method and Griddata V4 interpolation method only have certain errors in the low frequency region.

**Keywords:** large-span roof structure; proper orthogonal decomposition; wind tunnel test; wind-pressure field reconstruction; wind pressure coefficient



**Citation:** Su, Y.; Di, J.; Li, J.; Xia, F. Wind Pressure Field Reconstruction and Prediction of Large-Span Roof Structure with Folded-Plate Type Based on Proper Orthogonal Decomposition. *Appl. Sci.* **2022**, *12*, 8430. <https://doi.org/10.3390/app12178430>

Academic Editor: José A.F.O. Correia

Received: 11 August 2022

Accepted: 23 August 2022

Published: 24 August 2022

**Publisher's Note:** MDPI stays neutral with regard to jurisdictional claims in published maps and institutional affiliations.



**Copyright:** © 2022 by the authors. Licensee MDPI, Basel, Switzerland. This article is an open access article distributed under the terms and conditions of the Creative Commons Attribution (CC BY) license (<https://creativecommons.org/licenses/by/4.0/>).

## 1. Introduction

The large-span roof structure has many advantages such as various external forms and large internal space capacity. It can well meet the requirements of major cities for public buildings, resulting in its wide application and often as a local landmark building. It is also the practice of this type of architecture that promotes the innovation and development of spatial structures. The large-span roof structure has the characteristics of light weight, large flexibility, small damping, low natural vibration frequency, and dense mode shapes, and its main mode shapes are not concentrated in the first few orders like high-rise buildings, which makes it more sensitive to the effect of wind. Cases of wind-induced disasters caused by excessive wind force are not uncommon [1–4]. Therefore, it is of great significance to reasonably and effectively predict the wind load of the large-span roof structure to improve its wind resistance performance.

Due to the large spatial span of the large-span roof structure, there are often more effects such as vortex shedding and reattachment, the quasi-steady theory is no longer applicable, and the wind load is very complex [5–7]. Furthermore, due to its complex and diverse structural forms, neither the norm nor the design guideline can provide universal wind load calculation parameters such as body shape coefficient, which often need to be obtained through means like field measurement, numerical simulation, and wind tunnel test [8–12]. However, field measurement is rarely used because it has significant limitations such as being time-consuming and labor-consuming and having expensive and harsh conditions. Although numerical simulation has the advantages of low cost, short period, and few restrictions, the current method still has obvious difficulties in grid division, turbulence modeling, and computational efficiency, and the accuracy cannot be guaranteed, so it is not widely used. As an irreplaceable method in aerodynamic research, the wind tunnel test is the most common and effective method to obtain parameters such as body shape coefficient of large-span roof structure. Unfortunately, due to the limitations of the model and test conditions, the number of wind pressure measurement points in the test is very limited, and it is far from being able to accurately evaluate and predict the wind load of large-span roof structures. Therefore, it is very important to obtain the wind pressure information in the area without pressure measuring points more accurately and conveniently. At present, there are two conventional methods: one is to use the test results at the nearest measuring point as the wind load time history in the unknown area; the other is to increase the density of test results on the measuring points by spatial interpolation to obtain wind load time history data in the unknown areas. The former is obviously unreasonable. For the latter one, based on the limited wind tunnel test pressure measurement data, how to select a reasonable and effective processing method to improve the test data utilization rate and the wind load evaluation accuracy of large-span roof structures has become an urgent problem.

As a mathematical tool to analyze the statistical characteristics of complex random fields, the method of proper orthogonal decomposition (i.e., POD, also known as the Karhunen–Loève expansion) has been widely used in many fields [13–17]. In the field of stochastic wind field, the stochastic phenomenon is simplified by adopting the space-time separation technique in a new coordinate space, and the wind pressure field is decomposed into a series expansion of principal coordinates only related to time and eigenmodes only related to space. The eigenmodes at the points to be evaluated are predicted using a spatial interpolation method. Then combine them with the principal coordinates, and the wind pressure field can be approximately described with finite terms to simplify the distribution of the wind pressure field for simplified analysis. This method can obviously compress the data storage and accurately describe the essential characteristics of the wind pressure field with fewer items [18–21].

As early as 1967, Lumley introduced the POD method to the study of turbulence. Then the following year, Armit [22] took the lead in introducing the POD method to the field of wind engineering. After that, many scholars in the field adopted this method to describe the fluctuating wind pressure field of the architectural structure. Holmes [23] pointed out that because the shape of eigenvectors is restricted by the requirement of orthogonality, the interpretation of its physical meaning may be distorted. However, he also pointed out that the fluctuating wind pressure field can be simplified into several modes for analysis by POD method. Davenport [24] applied the POD method to the research of wind speed field and wind pressure field and proposed a method that can simplify the description of wind load. Bienkiewicz et al. [25,26] reconstructed the fluctuating wind field of a flat roof. Tamura [27] uses the POD method to describe the characteristics of wind pressure field in low-rise buildings. Chen [28] adopted a database strategy and used POD technology to predict the wind pressure field in the far distance by interpolation based on the wind pressure field in the corner of the roof and compared the interpolation results with the measured data in terms of statistical characteristics and power spectral density. In recent years, Li et al. and many other scholars [29–32] have expounded the application of POD technology in

the reconstruction of wind pressure fields such as curved roofs and double-slope roofs. Since then, POD has gained more attention and application as an effective tool that can accurately and simplify the description of the wind pressure field [18,19,33].

However, there has been no research on the reconstruction of wind pressure field for folded-plate large-span roof structures based on POD technology. Therefore, it is necessary to further explore the applicability and accuracy of the POD method and different spatial interpolation methods in the reconstruction and prediction of the wind pressure field of the folded-plate large-span roof structure. The structures with this type often have typical roof surfaces such as windward and leeward folded plates, side folded plates, and roof planes, which are representative to a certain extent. With this type of structure, the wind loads in different wind-receiving areas of large-span roof structures can be systematically analyzed. This paper will take a high-speed railway station with a folded-plate large-span roof as the engineering background. First, the rigid model pressure measurement of the structure is carried out through the wind tunnel test to obtain the wind pressure time series of the measuring points on the roof surface, and the parameters such as the mean wind pressure coefficient and the body shape coefficient are analyzed. Then, based on the POD method, the wind pressure field of the roof is reconstructed by using the first several eigenmodes of the structure, and it is compared with the wind tunnel test results in terms of statistical characteristics, power spectrum, coherence function, etc., to study the applicability and effectiveness of the POD method in the reconstruction of the random wind pressure field of the folded-plate roof. Finally, the POD method is used to predict the wind pressure of some unknown measuring points of the structure based on various interpolation methods, and the accuracy and difference of different interpolation methods in the wind pressure prediction of the large-span roof structure are compared and analyzed.

## 2. Proper Orthogonal Decomposition Theory

### 2.1. Spatial Projection Extremum Principle [34]

The fluctuating wind pressure of the point  $(x, y)$  at time  $t$  is  $P(x, y, t)$ , the proper orthogonal decomposition is performed on it, and the eigenmode  $\varphi(x, y)$  is found to maximize the projection of  $P(x, y)$  on it. At this time, the function  $\varphi(x, y)$  is most related to the wind pressure field, and

$$\int \int P(x, y, t)\varphi(x, y)dxdy = \max \tag{1}$$

Since the positive and negative of  $P(x, y, t)$  is uncertain, the mean square method is used to regularize the above equation:

$$\frac{\int \int P(x, y, t)\varphi(x, y)dxdy \int \int P(x', y', t')\varphi(x', y')dx'dy'}{\int \int \varphi^2(x, y)dxdy} = \frac{\int \int c(x, y, x', y')\varphi(x', y')dx'dy'}{\varphi(x, y)} = \max = \lambda \tag{2}$$

where  $c(x, y, x', y')$  is the covariance of any two points in the wind pressure field.

Because the data obtained from the wind tunnel test is a sequence of wind pressure time sequences of a series of discretely distributed measuring points, the above equation can be rewritten into discrete form:

$$\sum_{i=1}^N c(x, y, x', y')\varphi(x', y')\Delta A_i = \lambda\varphi(x, y) \tag{3}$$

where  $N$  is the number of measuring points of the pressure test;  $\Delta A_i$  is the calculated area corresponding to the  $i$ -th measuring point.

### 2.2. Rayleigh Quotient Derivation [35]

Assuming that  $P_i(t) = P_i(x_i, y_i, t)$  is the fluctuating wind pressure of point  $(x_i, y_i)$  at time  $t$ , and  $\{P(t)\} = \{P_1(t), P_2(t), P_3(t), \dots, P_N(t)\}^T$  is the time history of fluctuating wind pressure on the surface of the structure, its maximum projection is:

$$a_n(t) = \{P(t)\}^T \{\varphi\}_n = \{\varphi\}_n^T \{P(t)\}, \quad n = 1, 2, 3, \dots, N \tag{4}$$

where  $\{\varphi\}_n$  is a set of basis vectors in the orthogonal coordinate system.

Since the positive and negative of  $P(t)$  is uncertain, the mean square method is used to regularize the above equation:

$$\overline{a_n^2(t)} = \frac{\{\varphi\}_n^T \overline{\{P(t)\} \{P(t)\}^T} \{\varphi\}_n}{\{\varphi\}_n^T \{\varphi\}_n} = \frac{\{\varphi\}_n^T [c] \{\varphi\}_n}{\{\varphi\}_n^T \{\varphi\}_n} = \lambda_n \tag{5}$$

where  $[c]$  is the covariance matrix, and  $c_{ij} = \overline{P_i(t) P_j(t)}$ .

According to the property of Rayleigh quotient, the above Equation (5) obtains the standing value only when  $\{\varphi\}_n$  is the eigenvector of  $[c]$ , and the standing value is equal to the eigenvalue  $\lambda_n$ :

$$[c] \{\varphi\}_n = \lambda_n \{\varphi\}_n, \quad n = 1, 2, 3, \dots, N \tag{6}$$

Assuming that  $\{\varphi\}_n$  is orthogonal, the eigenvector and principal coordinate matrix are  $[\Phi] = [\{\varphi\}_1, \{\varphi\}_2, \dots, \{\varphi\}_n]$  and  $\{a(t)\} = \{a_1(t), a_2(t), \dots, a_n(t)\}$ , respectively, then the projection  $a_n(t)$  can be rewritten as:

$$\{a(t)\} = [\Phi]^T \{P(t)\} \tag{7}$$

Since  $[\Phi]$  is an orthogonal matrix, then:

$$\{P(t)\} = \left([\Phi]^T\right)^{-1} \{a(t)\} = [\Phi] \{a(t)\} = \sum_{n=1}^N a_n(t) \{\varphi\}_n \tag{8}$$

The above equation is the series expansion of expressing the fluctuating wind pressure as the principal coordinate  $a_n(t)$  related only to time and the eigenmode  $\{\varphi\}_n$  related only to space, which is an analysis method that separates time and space.

### 2.3. Reconstruction of Wind Pressure Field

Based on Equations (5) and (8), the mean square value of the fluctuating pressure can be obtained, which shows that the eigenvalue  $\lambda_n$  can describe the contribution of the eigenmode  $\{\varphi\}_n$  to the mean square value of the fluctuating wind pressure:

$$\sigma_h^2(y) = \int_0^{+\infty} S_h(y, k_1) dk_1 \tag{9}$$

$$\sum_{i=1}^N \overline{P^2(x_i, y_i, t)} = \sum_{n=1}^N \sum_{m=1}^N \overline{a_n(t) a_m(t)} \{\varphi\}_n^T \{\varphi\}_m = \sum_{n=1}^N \lambda_n \tag{10}$$

That is, the sum of the mean square values of the fluctuating wind pressure is equal to the sum of the eigenvalues. The numerical value of each eigenvalue reflects the amount of energy contained in the corresponding mode. Therefore, the cumulative contribution of energy of different order modes can be considered as a basis for selecting the number of modes and evaluating their accuracy. The energy proportion  $E_i$  of each order eigenmode and the total energy proportion  $E_{1\sim i}$  of the first  $i$  order eigenmodes are:

$$E_i = \frac{\lambda_i}{\sum_{n=1}^N \lambda_n}, \quad E_{1\sim i} = \frac{\sum_{n=1}^i \lambda_n}{\sum_{n=1}^N \lambda_n} \tag{11}$$

If the first  $M$  order energy ratios can meet the accuracy requirements when  $i = M$ , the first  $M$  eigenmodes can be used to reconstruct the wind pressure field:

$$P(x, y, t) = \sum_{n=1}^M a_n(t) \varphi_n(x, y) \quad (12)$$

According to the above-mentioned reconstruction of wind pressure field based on POD technology and through the idea of energy ratio of Equation (11), the wind pressure field can be well described by selecting a few order eigenmodes, which simplifies the analysis of fluctuating wind pressure. After the wind pressure field is reconstructed, the unknown point is interpolated by using the eigenmodes of the known position, and the wind pressure time histories of the unknown points can be predicted by Equation (12) [36–38].

### 3. Rigid Model Pressure Measurement Test

#### 3.1. Test Equipment

The rigid model pressure measurement test was carried out in the XNJD-3 wind tunnel of Southwest Jiaotong University. The wind tunnel is the largest boundary layer wind tunnel in the field of wind engineering in the world. The size of the test section is 36 m (length)  $\times$  22.5 m (width)  $\times$  4.5 m (height). The huge test section size enables pressure testing of the large-scale large-span roof models. The wind speed of the wind tunnel in the vacant state can be adjusted from 1.0 to 16.5 m/s, and the turbulent intensity of the incoming flow is less than 1%, and the average airflow deflection angles in both the longitudinal and vertical directions are less than  $1^\circ$  [39–41].

The turbulent wind field characteristics were collected using the TFI Cobra three-dimensional fluctuating anemometer (Figure 1a). Its measuring linear frequency range is 0~2000 Hz, the measurable wind speed range is 2~100 m/s, and the allowable error of measuring wind speed is  $\pm 0.1$  m/s. Wind pressure measurement adopted Scanivalve DSM4000 electronic pressure scanning valve system (Figure 1b). The system converts pressure signals into electrical signals, which are amplified and sent back to the pressure acquisition system, and then the pressure values of each circuit are collected and stored by the computer. The system can realize the synchronous acquisition of dynamic pressure signals of several measuring points, the measuring range is 0~ $\pm 2000$  Pa, and the measuring accuracy is  $\pm 0.08\%$  of the full scale [42,43].



**Figure 1.** Test data acquisition device: (a) TFI Cobra three-dimensional fluctuating anemometer; (b) Scanivalve DSM4000 electronic pressure scanning valve system.

#### 3.2. Turbulence Field Simulation and Model Production

In the wind tunnel, an atmospheric boundary layer passive simulation device composed of minarets, baffles, and floor roughness elements was used to simulate the turbulent fluctuating characteristics. The length of the device on the wind tunnel floor was approximately 25 m, which ensures the generation of reasonably accurate turbulence fields. According to the Code for Loads of Building Structures [44] and combined with the loca-

tion of the structure, the simulated ground roughness coefficient in the test was taken as  $\alpha = 0.15$ .

The large-span roof structure is 304 m long, 208 m wide, and 40 m high. Considering the size of the wind tunnel test section and the actual size of the building, the scale ratio was set to 1:100. The blocking rate of the model in the wind tunnel was less than 5%, which meets the test requirements.

The pressure measurement model was made of composite materials and plexiglass, and the pseudo-model and the characteristic buildings around the structure are simulated with foam plastic. The test photos are shown in Figure 2.



**Figure 2.** Wind tunnel test for rigid model pressure measurement: (a) front view; (b) side view.

### 3.3. Measuring Point Layout and Test Conditions

The large-span roof structure is divided into the first phase and the second phase, and the two parts of the building are centrally symmetrical (the pressure measurement model and the pseudo model in Figure 2). Therefore, only half of the structure was selected for the measuring point arrangement and data processing in the test. Because the roof is large and complicated in form, in order to facilitate the measurement, the pressure test was carried out after the roof was zoned. A total of 2010 measuring points were arranged on the structure, of which 1402 measuring points were arranged in the roof part. The layout of the roof surface zoning and measuring points is shown in Figure 3.

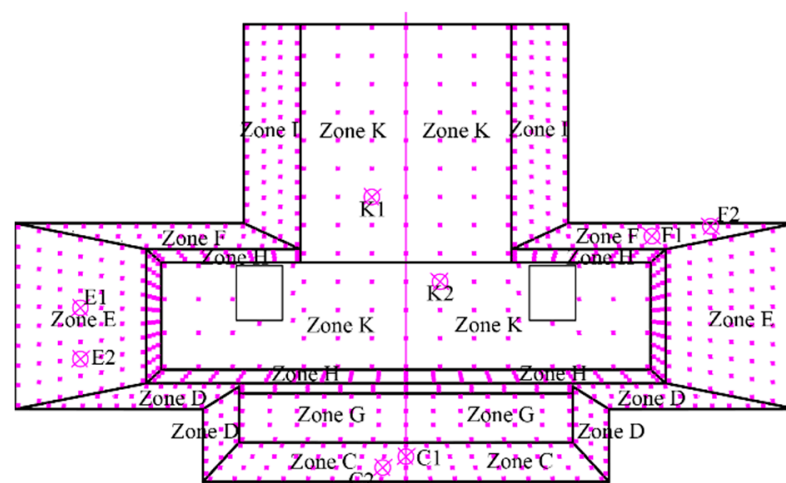


**Figure 3.** Layout of zoning and wind pressure measuring points on roof surface.

According to the layout of the wind pressure measuring points, the drill tool was used to drill the corresponding points. One end of the extremely tough rubber tubes was glued to the model, and tools such as blades were used to flatten the surface of the model. The other end of the rubber tubes was connected to the pressure measuring line of the scan

valve. Finally, each scanning valve was connected to the corresponding channel on the collecting box.

Before the formal test, the wind pressure collection data under no wind were checked to ensure that the collection equipment is in normal working condition. A total of 24 working conditions were selected for the test wind direction angle. A test wind direction angle was set every 15° from 0° to 345°, i.e.,  $\Delta\alpha = 15^\circ$ . The incoming flow direction directly in front of the railway station square was defined as  $\beta = 0^\circ$ , as shown in Figure 4. The test reference point was taken at the height of the roof top surface (about 43 cm). According to the basic wind speed of the city and region where the structure is located, the wind speed was 8 m/s. Comprehensively taking into account the frequency setting of the acquisition equipment and the effectiveness of data processing, the sampling frequency was 200 Hz, and the sampling time was 60 s.

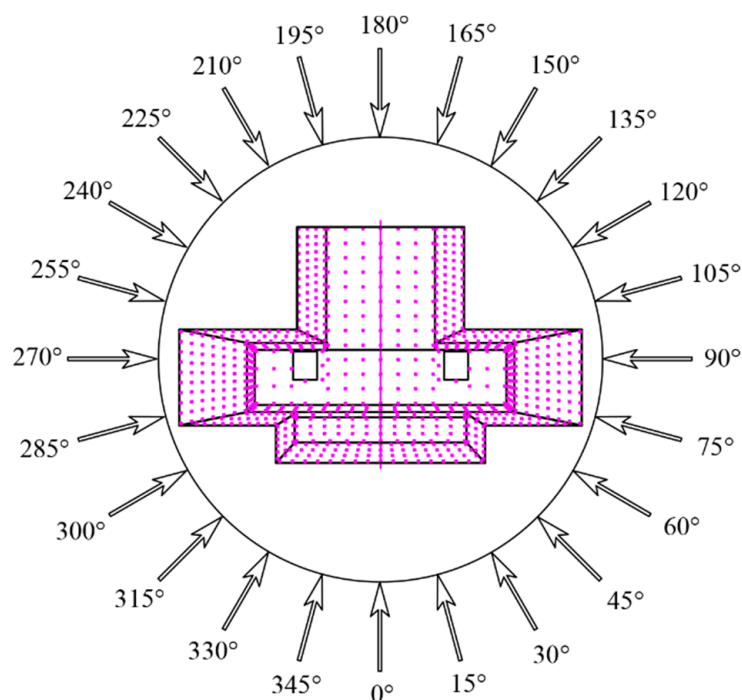


**Figure 4.** Schematic diagram of the test wind direction angle.

In the test, the Scanivalve DSM4000 electronic pressure scanning valve system was used to collect the pressure synchronously at the wind pressure measuring points on the roof surface. Data were checked after repeating the measurement twice for each test condition to avoid failed data acquisitions. In addition, before the test of each group of working conditions was carried out, there will be a few minutes of waiting before the collection to make the flow field reach a stable state and reduce the measurement error.

### 3.4. Data Processing Method

The wind pressure field is usually analyzed by using the wind pressure coefficient. Its advantage is that the coefficient is dimensionless, and the wind pressure coefficient of the corresponding point on the actual structure and the test model is the same, which brings convenience to the analysis. The research of this paper aims to analyze the effectiveness and accuracy of POD technology in the reconstruction of wind pressure field of large-span folded-plate roof. The wind pressure coefficient is used as a very effective tool parameter. According to the pressure time history of each measuring point obtained by the test, the mean wind pressure coefficient of the corresponding measuring point can be obtained:

$$C_{\bar{P}_i} = \frac{\bar{P}_i - \bar{P}_\infty}{\bar{P}_0 - \bar{P}_\infty} \tag{13}$$

where  $C_{\bar{P}_i}$  is the mean wind pressure coefficient of the  $i$ -th measuring point;  $\bar{P}_i$  is the mean pressure value of the  $i$ -th measuring point;  $\bar{P}_0$  and  $\bar{P}_\infty$  are the mean total pressure and static pressure at the reference height at infinity, respectively.

### 3.5. Test Results and Analysis

The mean wind pressure coefficient of each measuring point on the roof can be calculated by Equation (13), and the contour map of the coefficients on the roof can be drawn, which can reflect the overall wind pressure distribution and law on the roof surface. Due to the large number of test conditions and the huge amount of data, only the results under 6 characteristic wind direction angles are selected for display, as shown in Figure 5.

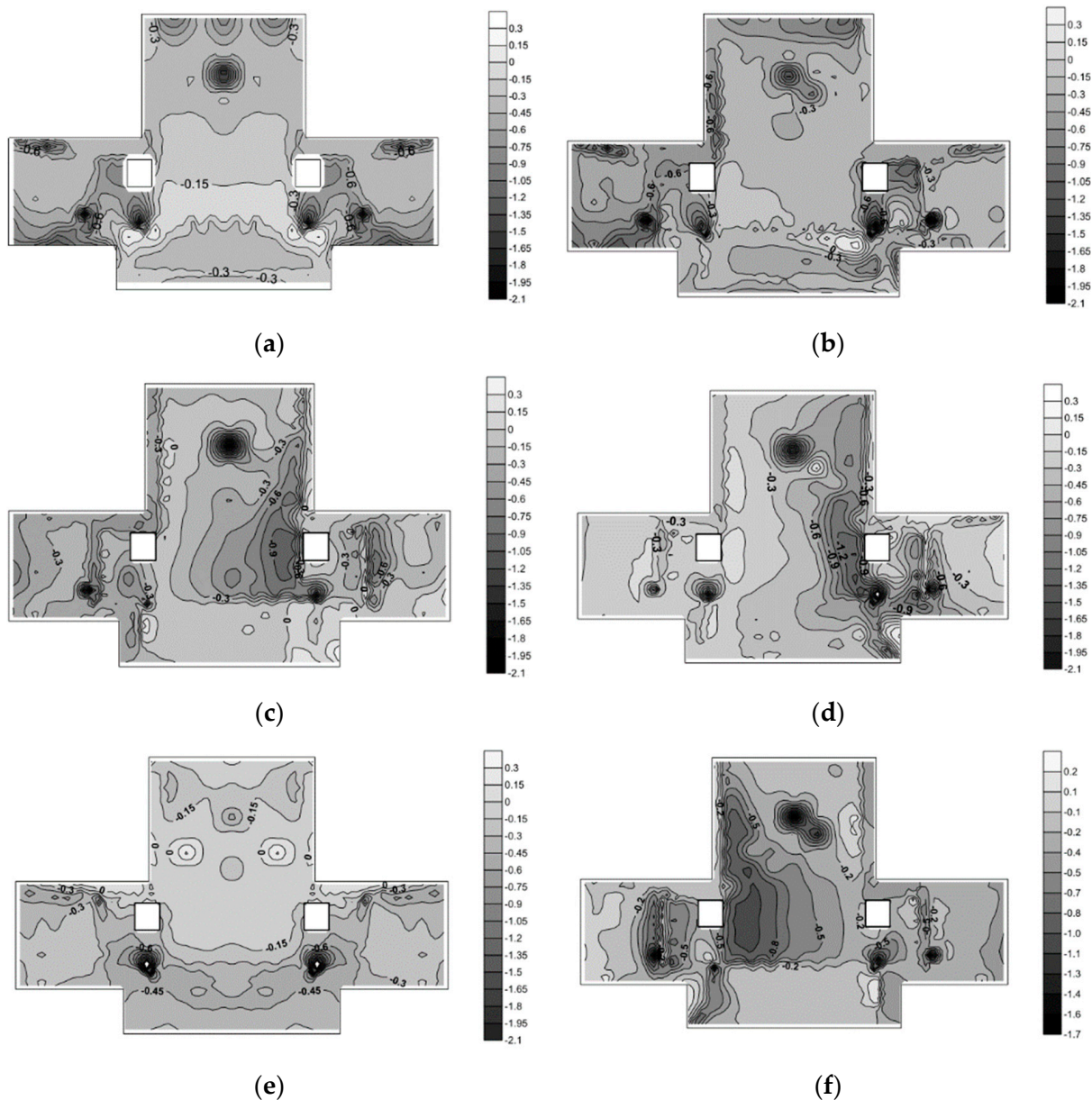


**Figure 5.** The contour map of the mean wind pressure on the roof under the characteristic wind direction angle: (a) 0° wind direction angle; (b) 45° wind direction angle; (c) 90° wind direction angle; (d) 135° wind direction angle; (e) 180° wind direction angle; (f) 270° wind direction angle.

According to Figure 5, it can be found that: (1) The flow separation phenomenon will occur at the edge of the roof, and the negative inclination angle delays the reattachment phenomenon, so that under the action of any wind direction angle, the mean wind pressure

coefficients of the roof are mainly negative. The mean wind pressure coefficients of the folded plate surface with a negative inclination angle are all negative in the downwind, while the coefficients of the folded plate surface with a positive inclination angle have positive values in some areas, but the positive pressure value is very small, that is, the roof is mainly subjected to upward lift under different wind direction angles. (2) The leading edge of the roof in the direction of the incoming flow and the position where the structural form changes abruptly will greatly disturb the incoming flow, causing the flow direction to change abruptly, resulting in a clear distinction of the intensity of the contour map. The mean wind pressure coefficients around the openings on both sides of the roof and at the edge of the roof varies greatly. (3) The structural forms which the incoming flow run through are inconsistent, which makes the mean wind pressure coefficients at any point change greatly under different wind direction angles. In addition, due to the existence of characteristic buildings around the station and the inconsistency of the heights of platforms and canopies on both sides of the station, the wind pressure results under the conditions of symmetrical wind direction angles do not show strict axis symmetry.

For the structural wind pressure measurement test and results in this section, we need to make the following descriptions. Firstly, each group of measurements was performed twice, and the next test was only continued after ensuring that the data were correct. Secondly, in the research of this paper, a number of typical measuring points in different zones were selected to conduct a systematic study, which effectively avoided the occasionality of analysis. Even so, there were inevitably some errors in the results due to the influence of experimental techniques and other factors. In order to make the evaluation of the wind pressure field on the roof surface more precise, more measuring points were often selected in the test. Unfortunately, due to the limited measurement channels on current pressure acquisition devices, multiple acquisitions had to be performed. This made the wind pressure of each measuring point on the roof unable to be collected synchronously, which brought certain errors to the wind pressure field evaluation and reconstruction analysis. In addition, due to the large size of the structure and model, the pressure measuring pipeline was long in the test. Many studies showed that the long pressure measuring pipeline causes a little loss of the actual fluctuating wind pressure on the roof surface and causes errors. In view of the above problems, on the basis of limited equipment conditions, it is necessary to further analyze the importance of each error influencing factor and weigh and select a more reasonable test plan.

#### 4. Reconstruction of Wind Pressure Field on Roof Surface

In view of the large span of the roof, there are many measuring points, and the wind pressure coefficients vary widely. For the convenience of analysis, the wind pressure field of the roof was reconstructed according to the measuring zone of the wind tunnel test. Due to the large amount of data, this paper takes the wind direction angle of  $0^\circ$  as an example and selects four typical zones, zone C (windward folded plate), zone E (side folded plate), zone F (leeward folded plate), zone K (roof flat plate), and analyzes the wind pressure field reconstruction based on the POD method for each area, respectively.

##### 4.1. Energy Ratio Analysis

In order to analyze and show the influence of the mean value of wind pressure on the results in the reconstruction analysis of the wind pressure field on the roof surface using the POD method, based on the mean wind pressure (including the mean value of wind pressure on the roof surface) and the fluctuating wind pressure (excluding the mean value of wind pressure on the roof surface), the correlation matrix of wind pressure coefficients in each zone was analyzed through POD method. From the perspective of energy ratio of Equation (11), the cumulative energy ratio of each eigenmode is shown in Figure 6.

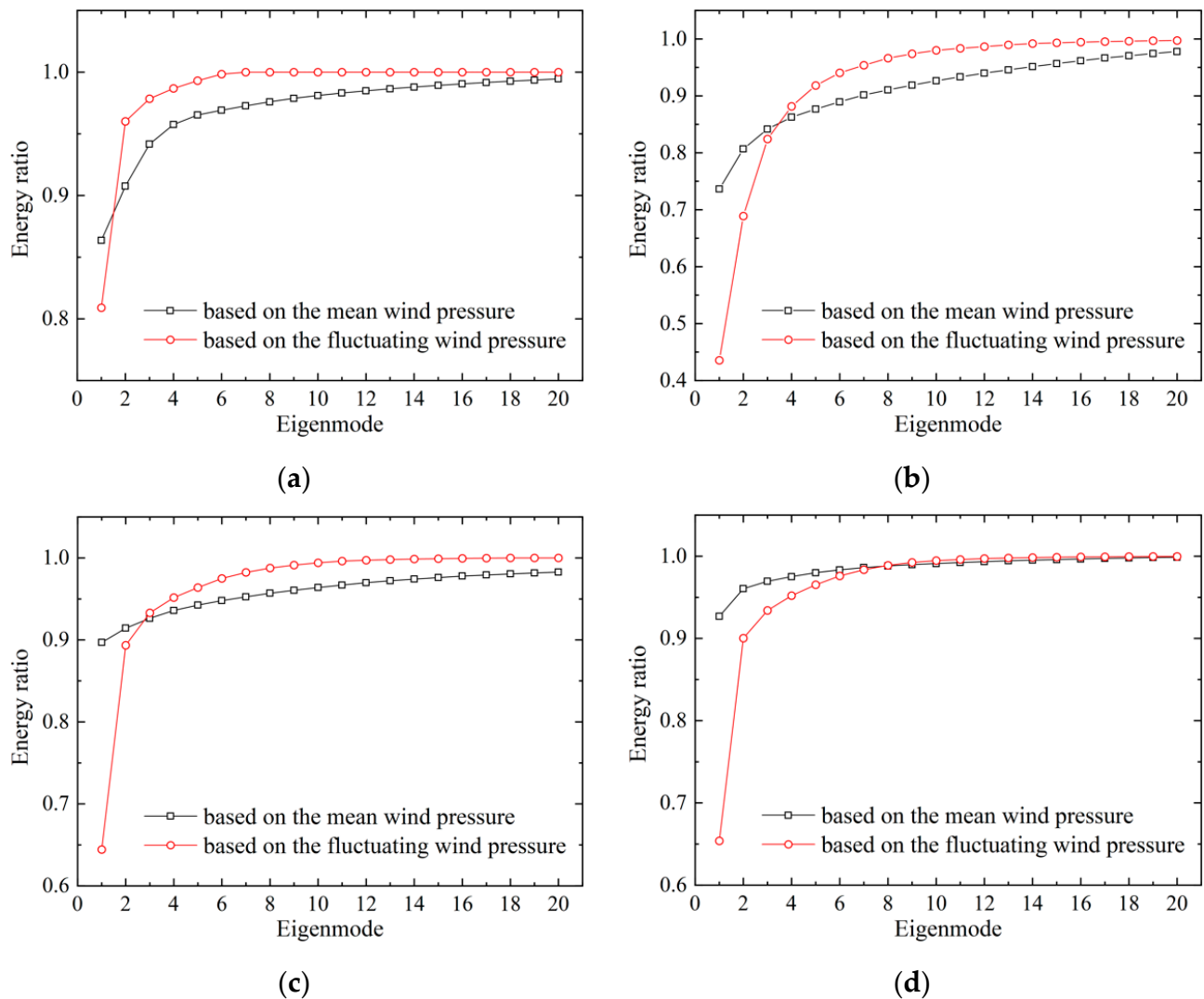


**Figure 6.** Cumulative energy ratio of eigenmodes in each zone: (a) zone C; (b) zone E; (c) zone F; (d) zone K.

It can be seen from the figure that the modal energy ratio of the reconstruction based on the fluctuating wind pressure in each zone is smaller than that of the reconstruction based on the mean wind pressure in the first order, but the former quickly approaches 1 and is close to the full energy. However, in the wind field reconstruction based on the mean wind pressure, the convergence rate of the cumulative modal energy to the true energy is much slower. In addition, the convergence rate of the windward folded plate (zone C), the leeward folded plate (zone F), and the roof flat plate (zone K) is relatively fast, and the rate of the side folded plate (zone E) is relatively slow. Despite the above phenomena, the energy ratios of the first few orders in each zone in the two reconstruction results are very large. The cumulative energy ratios of the first five orders can basically reach more than 90%, and that of the first 20 orders can reach more than 95%, which can realize the restoration of the real wind pressure field energy with high precision.

#### 4.2. Statistical Value Analysis

Based on Equation (12), different eigenmode orders were selected to decompose the wind pressure field. Four feature points (named C1, E1, F1, and K1) were selected from the four zones C, E, F, and K, respectively, and analyzed by the root mean square (RMS) value. The results are shown in Tables 1 and 2.

**Table 1.** RMS value of wind pressure at each measuring point in the reconstructed wind field (based on mean wind pressure).

Measuring Point	Test Value	5 Eigenmode Orders		10 Eigenmode Orders		20 Eigenmode Orders	
		Reconstructed Value	Error	Reconstructed Value	Error	Reconstructed Value	Error
C1	0.453	0.427	5.6%	0.440	2.9%	0.448	1.1%
E1	0.218	0.188	13.7%	0.199	8.7%	0.210	3.7%
F1	0.525	0.483	7.9%	0.496	5.5%	0.511	2.1%
K1	0.258	0.251	2.7%	0.253	2.0%	0.256	0.3%

**Table 2.** RMS value of wind pressure at each measuring point in the reconstructed wind field (based on fluctuating wind pressure).

Measuring Point	Tested Value	5 Eigenmode Orders		10 Eigenmode Orders		20 Eigenmode Orders	
		Reconstructed Value	Error	Reconstructed Value	Error	Reconstructed Value	Error
C1	808.5	789.7	2.3%	801.8	0.08%	808.5	0.0%
E1	428.0	391.4	8.6%	417.6	2.4%	427.2	0.02%
F1	276.5	265.3	4.0%	272.5	1.4%	276.5	0.007%
K1	286.7	273.2	4.7%	280.5	2.1%	286.6	0.04%

It can be seen from the tables that with the increase of the selected eigenmode order, the wind pressure field reconstruction result is closer to the true value, and when 20 eigenmode orders are selected, a good approximation to the actual wind field can be achieved in terms of statistical value. On the other hand, the reconstruction results based on fluctuating wind pressure converge much faster than those based on mean wind pressure, and a good approximation of the wind field can be achieved in the 10th order, which is consistent with the energy ratio analysis in the previous section. In addition, combined with the analysis of the cumulative energy ratio of each zone, it is found that the reconstruction effect of the wind pressure field based on the POD method is related to the spatial position of the predicted point, and the overall performance is that the wind field reconstruction effect on the windward folded plate (zone C), the leeward folded plate (zone F), and the roof flat plate (zone K) is obviously better than that on the side folded plate (zone E).

#### 4.3. Power Spectrum Analysis

The power spectrum represents the variation of signal power with frequency, that is, the distribution of signal power in the frequency domain. Based on the aforementioned analysis of energy ratio and statistical values, the aforementioned four feature points were still used for analysis, and the reconstruction results of the first 20 eigenmodes were selected to show the power spectrum situation. In the analysis of the first two sections, when the 20 eigenmode orders were selected for wind field reconstruction, the reconstruction based on mean wind pressure and fluctuating wind pressure both could achieve high-precision simulation of wind pressure field, and the error was extremely small. Therefore, only the reconstruction results based on the mean wind pressure are shown in this section, as shown in Figure 7.

It can be seen from Figure 7 that the reconstructed wind pressure power spectral densities of the typical measuring points in the four zones are in good agreement with the test results. The power spectrum analysis results show that the effect is very good when the first 20 eigenmodes are used to reconstruct the wind pressure field.

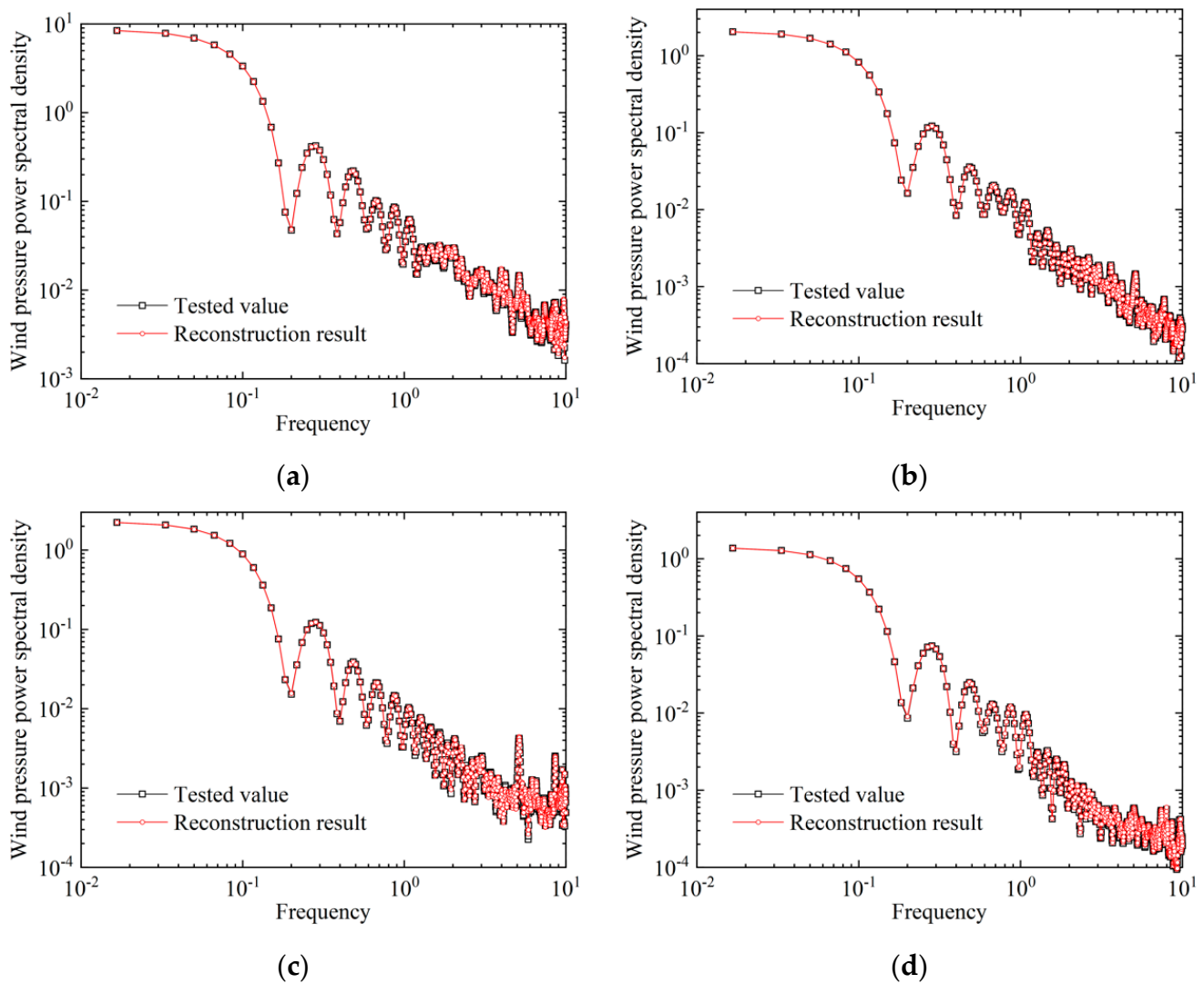


**Figure 7.** Wind pressure power spectral density of reconstructed wind field: (a) feature point C1; (b) feature point E1; (c) feature point F1; (d) feature point K1.

4.4. Correlation Analysis

Correlation is a very important statistical parameter in the field of research, which characterizes the degree of correlation between the measuring values of the same measuring point at different times or different measuring points at the same time. In this section, the coherence function is used to describe the correlation between the test and the reconstructed wind pressure field, as shown in Figure 8.

As can be seen from the figure, the coherence function value is close to 1 except that it is near 0.97 in the high frequency part in zone F. It shows that when the 20 eigenmodes were used to reconstruct the wind pressure field, the wind pressure coefficient correlation between the time history of the test and the reconstructed wind field is extremely high, and the reconstruction result of the wind pressure field is very accurate.

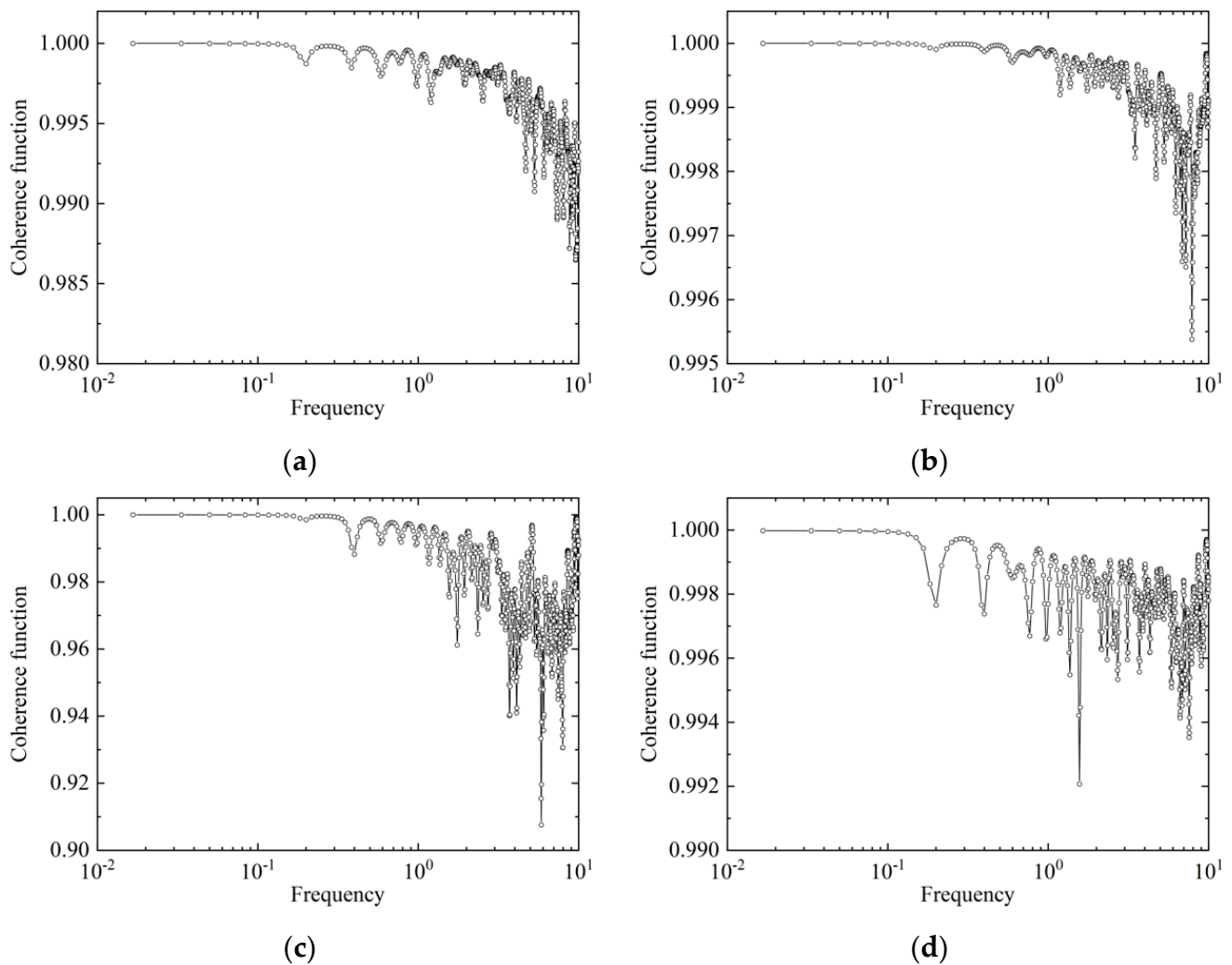


**Figure 8.** Coherence function between test and reconstructed wind pressure coefficients: (a) feature point C1; (b) feature point E1; (c) feature point F1; (d) feature point K1.

## 5. Wind Pressure Field Prediction

Based on the above Equation (12), the POD method can be used to predict the wind pressure of the points that are not arranged in the test. That is, by predicting the eigenmode of the point and taking the principal coordinates used in the prediction, the prediction of the wind pressure at this point can be realized. The specific scheme is as follows: since the eigenmode is only related to the spatial position of the measuring point and has nothing to do with other variables, the eigenmode of the point can be interpolated according to the spatial position relationship between the predicted point and the surrounding known measuring points, and then, combined with the main coordinates, the wind pressure time history of the predicted point can be obtained according to Equation (12). In this paper, C2, E2, F2, and K2 were selected as unknown points. A variety of existing commonly used interpolation methods were used: adjacent point interpolation method, bilinear interpolation method, bicubic interpolation method, and Griddata V4 interpolation method, respectively, predicted the eigenmodes and wind pressure of unknown points. Finally, the results were compared with the test values.

### 5.1. Statistical Value Analysis

According to the wind field reconstruction results based on the mean wind pressure in the previous section, the 20 eigenmodes were used to predict the wind pressure at the

unknown points, and the eigenmodes of predicted points were calculated by different interpolation methods, and then, the time histories of the wind pressure coefficients at the predicted points were obtained. The mean value and the RMS value were compared with the time history of the test wind pressure coefficient, and the results are shown in Tables 3–6.

**Table 3.** Statistical value and error of wind pressure coefficient at predicted point C2.

	<b>Tested Value</b>	<b>Adjacent Point Method</b>	<b>Bilinear Method</b>	<b>Bicubic Method</b>	<b>Griddata V4 Method</b>
Mean value	−0.245	−0.231	−0.234	−0.238	−0.237
Error of mean value		−5.7%	−4.5%	−2.8%	−3.2%
RMS value	0.315	0.283	0.322	0.300	0.339
Error of RMS value		−10.2%	2.2%	−4.8%	7.6%

**Table 4.** Statistical value and error of wind pressure coefficient at predicted point E2.

	<b>Tested Value</b>	<b>Adjacent Point Method</b>	<b>Bilinear Method</b>	<b>Bicubic Method</b>	<b>Griddata V4 Method</b>
Mean value	−0.429	−0.285	−0.394	−0.323	−0.366
Error of mean value		−33.6%	−8.1%	24.7%	14.7%
RMS value	0.242	0.301	0.226	0.240	0.254
Error of RMS value		24.4%	−6.6%	−0.7%	5.0%

**Table 5.** Statistical value and error of wind pressure coefficient at predicted point F2.

	<b>Tested Value</b>	<b>Adjacent Point Method</b>	<b>Bilinear Method</b>	<b>Bicubic Method</b>	<b>Griddata V4 Method</b>
Mean value	−0.416	−0.368	−0.378	−0.380	−0.393
Error of mean value		−11.5%	−9.0%	−8.6%	−5.4%
RMS value	0.269	0.209	0.255	0.246	0.251
Error of RMS value		−22.4%	−5.2%	−8.6%	−6.8%

**Table 6.** Statistical value and error of wind pressure coefficient at predicted point K2.

	<b>Tested Value</b>	<b>Adjacent Point Method</b>	<b>Bilinear Method</b>	<b>Bicubic Method</b>	<b>Griddata V4 Method</b>
Mean value	−0.207	−0.216	−0.215	−0.218	−0.270
Error of mean value		4.3%	3.9%	5.6%	30.8%
RMS value	0.244	0.235	0.240	0.272	0.337
Error of RMS value		−3.8%	−1.6%	11.4%	38.3%

According to the above tables, it can be seen that for the measuring points in zone K, the most ideal prediction effect is from the adjacent point interpolation method and the bilinear interpolation method. For the measuring points in zones C, E, and F, the bilinear method, the bicubic method and the Griddata V4 method are all ideal. The reason may be that the zone K belongs to the plane zone; the zones C, E, F belong to the three-dimensional zone; and the adjacent point interpolation has a better effect on the two-dimensional space, the last three methods have higher accuracy for the three-dimensional space interpolation. It can be seen that, based on the analysis of statistical values, the bilinear interpolation method has relatively better adaptability.

## 5.2. Power Spectrum Analysis

The measuring points in typical zones were selected, and the wind pressure power spectral densities of predicted points obtained by different interpolation methods were compared with the test results, as shown in Figure 9.

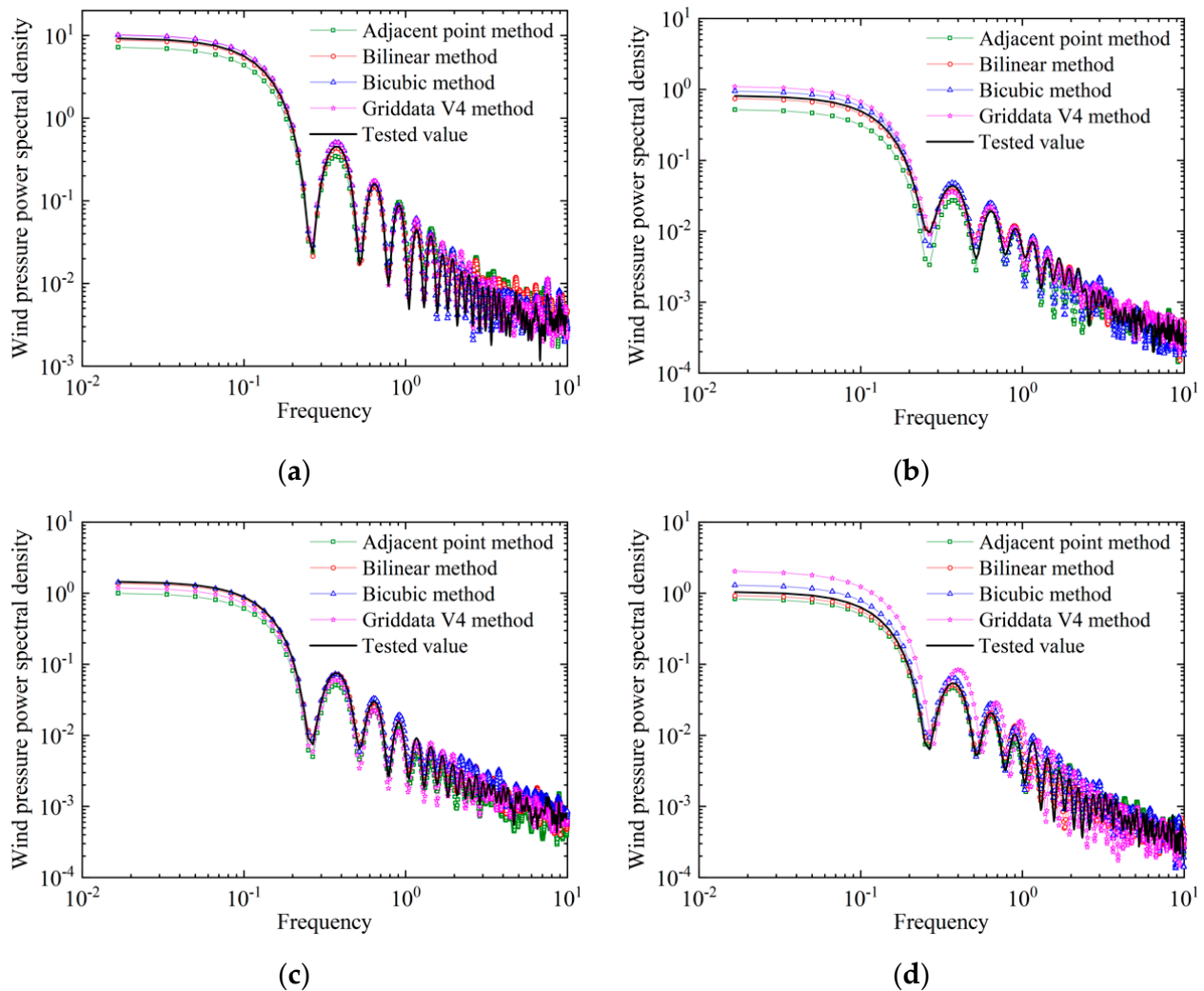


**Figure 9.** Wind pressure power spectral density of predicted points: (a) predicted point C2; (b) predicted point E2; (c) predicted point F2; (d) predicted point K2.

As shown in Figure 9, from the perspective of the wind pressure power spectral density at the predicted points, within a certain error range, the surface wind pressure of the large-span roof structure is predicted with good accuracy based on the above four different interpolation methods. The overall error of the windward folded plate (C2) is the smallest, followed by the leeward folded plate (F2), and the side folded plate (E2) and the roof flat plate (K2) have larger errors than the former two. Among the four interpolation methods, the bilinear method and the bicubic method have the highest accuracy, and both have very small errors with the test results in different zones. Except for zone C, the prediction results of the adjacent point method and the Griddata V4 method have certain differences with the test results in the low-frequency region. The prediction results of the former are generally smaller than the test results, especially in zone E of the side folded plate; the latter has a large error in zone K of the roof flat plate, and the predicted results are significantly larger than the test results.

### 5.3. Correlation Analysis

It should be noted that the wind pressure coherence functions of predicted points obtained based on different interpolation methods are all close to 1 in the low-frequency region and have large discreteness in the high-frequency region, the difference in prediction accuracy based on different interpolation methods is difficult to reflect. Therefore, the correlation coefficient is used in this section to describe the correlation between the wind

pressure time history predicted based on different interpolation methods and the test results. The results are shown in Table 7.

**Table 7.** Correlation coefficients between the wind pressure coefficients predicted based on different interpolation methods and the test values at predicted points.

	Adjacent Point Method	Bilinear Method	Bicubic Method	Griddata V4 Method
Predicted point C2	0.903	0.939	0.933	0.902
Predicted point E2	0.799	0.846	0.841	0.814
Predicted point F2	0.831	0.887	0.882	0.839
Predicted point K2	0.809	0.864	0.854	0.821

As can be seen from the above table, from the perspective of correlation, the bilinear method and the bicubic method have relatively higher accuracy, and they are still reliable interpolation methods. In the four selected zones, the accuracy results are similar to the analysis results of the previous two sections. The overall error of the windward folded plate (C2) is the smallest, and the correlation coefficients are all above 0.9; the relative error of the side folded plate (E2) is relatively large.

## 6. Conclusions

Taking a large-span roof with folded plate type as the background, this paper selected the first several eigenmodes of the structure and reconstructed the wind pressure field on the roof surface through the POD method. The statistical characteristics of the reconstructed wind pressure field were compared with the test measurement results, and the following main conclusions were drawn:

- (1) With the increase of the selected order of structural eigenmodes, the wind pressure field reconstruction results are closer to the true value. The actual wind field can be reconstructed with basically more than 90% accuracy when 5 eigenmode orders are selected, and the reconstruction can reach more than 95% accuracy when 20 eigenmode orders are selected.
- (2) The wind pressure field reconstruction effect based on the POD method is related to the spatial position of the predicted point. In general, the wind field reconstruction effect on the windward folded plate is better than that on the leeward folded plate, which is better than that on the roof flat plate and side folded plate. In addition, the effect of wind field reconstruction based on fluctuating wind pressure is better than that based on mean wind pressure.
- (3) By performing spatial interpolation of eigenmodes on the unknown points, the wind pressure time history of an unknown point of the structure can be effectively predicted based on the POD method. Different interpolation methods all can achieve relatively ideal results. Among them, the bilinear interpolation method has the highest accuracy, and the adjacent point interpolation method and Griddata V4 interpolation method only have certain errors in the low-frequency region.

In general, for the large-span roof structure with folded plate type, selecting reasonable structural eigenmode orders, the wind pressure field of the structure can be better reconstructed and predicted based on POD technology, which can provide effective technical support for the research and analysis of wind load on this type of large-span roof structures.

**Author Contributions:** Conceptualization, Y.S. and J.D.; methodology, Y.S. and J.D.; experiments, Y.S. and F.X.; validation, Y.S. and J.D.; investigation, Y.S., J.L. and F.X.; data curation, J.L. and F.X.; writing—original draft, Y.S.; writing—review and editing, Y.S. and J.L.; supervision, J.D.; funding acquisition, J.D. All authors have read and agreed to the published version of the manuscript.

**Funding:** This work was financially supported by the National Natural Science Foundation of China (51978108, 52008357).

**Institutional Review Board Statement:** Not applicable.

**Informed Consent Statement:** Not applicable.

**Data Availability Statement:** Data are contained within this article.

**Acknowledgments:** The authors thank the reviewers for their great help on the article during its review progress.

**Conflicts of Interest:** The authors declare no conflict of interest.

## References

1. Xuan, Y.; Xie, Z.; Zhang, L.; Li, Q. Estimation method of wind-induced fatigue of metal roof claddings under typhoon: Numerical analysis and experimental comparison. *Appl. Sci.* **2022**, *12*, 6785. [[CrossRef](#)]
2. Gavanski, E.; Nishimura, H. Wind loads on multi-span roof buildings. *J. Wind Eng. Ind. Aerody.* **2022**, *220*, 104824. [[CrossRef](#)]
3. Killen, G.P.; Letchford, C.W. A parametric study of wind loads on grandstand roofs. *Eng. Struct.* **2001**, *23*, 725–735. [[CrossRef](#)]
4. Zhang, G.; Zhang, Q.; Fan, F.; Shen, S. Research on snow load characteristics on a complex long-span roof based on snow-wind tunnel tests. *Appl. Sci.* **2019**, *9*, 4369. [[CrossRef](#)]
5. Simiu, E.; Scanlan, R.H. *Wind Effects on Structures*; John Wiley & Sons: New York, NY, USA, 1996.
6. Ogawa, T.; Nakayama, M.; Murayama, S.; Sasaki, Y. Characteristics of wind pressures on basic structures with curved surfaces and their response in turbulent flow. *J. Wind Eng. Ind. Aerody.* **1991**, *38*, 427–438. [[CrossRef](#)]
7. Ding, Z.; Tamura, Y. Contributions of wind-induced overall and local behaviors for internal forces in cladding support components of large-span roof structure. *J. Wind Eng. Ind. Aerody.* **2013**, *115*, 162–172. [[CrossRef](#)]
8. Fiouz, A.; Karbaschi, M.E. Effect of wind loading on spherical single layer space truss steel domes. *Int. J. Phys. Sci.* **2012**, *7*, 2493–2505.
9. Fu, J.; Xie, Z.; Li, Q.S. Equivalent static wind loads on long-span roof structures. *J. Struct. Eng.* **2008**, *134*, 1115–1128. [[CrossRef](#)]
10. Cheng, X.; Huang, G.; Yang, Q.; Zhou, X. Influence of Architectural Facades on Wind Pressures and Aerodynamic Forces of Tall Buildings. *J. Struct. Eng.* **2021**, *147*, 04020303. [[CrossRef](#)]
11. Kim, Y.C.; Yoon, S.W.; Cheon, D.J.; Song, J.Y. Characteristics of wind pressures on retractable dome roofs and external peak pressure coefficients for cladding design. *J. Wind Eng. Ind. Aerody.* **2019**, *188*, 294–307.
12. Huang, G.; Jiang, Y.; Peng, L.; Solari, G.; Liao, H.; Li, M. Characteristics of intense winds in mountain area based on field measurement: Focusing on thunderstorm winds. *J. Wind Eng. Ind. Aerody.* **2019**, *190*, 166–182. [[CrossRef](#)]
13. Kareem, A. Analysis and modelling of wind effects: Numerical techniques. *Wind. Eng. 21st Century* **1999**, *1*, 43–54.
14. Nejad, A.Z.B.; Mahmoudi, M. A POD-based methodology for structural finite element model updating. *J. Sound Vib.* **2022**, *534*, 117045. [[CrossRef](#)]
15. Litvinov, I.; Sharaborin, D.; Gorelikov, E.; Dulin, V.; Shtork, S.; Alekseenko, S.; Oberieithner, K. Modal decomposition of the precessing vortex core in a hydro turbine model. *Appl. Sci.* **2022**, *12*, 5127. [[CrossRef](#)]
16. Chen, M.; Liu, S.; Sun, S.; Liu, Z.; Zhao, Y. Rapid reconstruction of simulated and experimental temperature fields based on proper orthogonal decomposition. *Appl. Sci.* **2020**, *10*, 3729. [[CrossRef](#)]
17. Dessi, D.; Faiella, E. Modal parameter estimation for a wetted plate under flow excitation: A challenging case in using POD. *J. Sound Vib.* **2019**, *449*, 214–234. [[CrossRef](#)]
18. Wolter, C.; Trindade, M.A.; Sampaio, R. Obtaining mode shapes through the Karhunen-Loève expansion for distributed-parameter linear systems. *Shock Vib.* **2002**, *9*, 177–192. [[CrossRef](#)]
19. Kerschen, G.; Feeny, B.F.; Golinval, J.C. On the exploitation of chaos to build reduced-order models. *Comput. Method. Appl. Mech. Eng.* **2003**, *192*, 1785–1795. [[CrossRef](#)]
20. Huang, G. Application of proper orthogonal decomposition in fast Fourier transform-assisted multivariate nonstationary process simulation. *J. Eng. Mech.* **2015**, *141*, 04015015. [[CrossRef](#)]
21. Peng, L.; Huang, G.; Chen, X.; Kareem, A. Simulation of multivariate nonstationary random process: Hybrid stochastic wave and proper orthogonal decomposition approach. *J. Eng. Mech.* **2017**, *143*, 04017064. [[CrossRef](#)]
22. Armitt, J. *Eigenvector Analysis of Pressure Fluctuations on the West Burton Instrumented Cooling Tower*; Internal Report; Central Electricity Research Laboratories: Leatherhead, UK, 1968; pp. 114–168.
23. Holmes, J.D. Analysis and synthesis of pressure fluctuations on bluff bodies using eigenvectors. *J. Wind Eng. Ind. Aerody.* **1990**, *33*, 219–230. [[CrossRef](#)]
24. Davenport, A.G. How can we simplify and generalize wind loads? *J. Wind Eng. Ind. Aerody.* **1995**, *54*, 657–669. [[CrossRef](#)]
25. Bienkiewicz, B.; Ham, H.J.; Sun, Y. Proper orthogonal decomposition and reconstruction of roof pressure. *J. Wind Eng. Ind. Aerody.* **1993**, *50*, 193–202. [[CrossRef](#)]
26. Bienkiewicz, B.; Tamura, Y.; Ham, H.J.; Ueda, H.; Hibi, K. Proper orthogonal decomposition and reconstruction of multi-channel roof pressure. *J. Wind Eng. Ind. Aerody.* **1995**, *54*, 369–381. [[CrossRef](#)]
27. Tamura, Y.; Suganuma, S.; Kikuchi, H.; Hibi, K. Proper orthogonal decomposition of random wind pressure field. *J. Fluids Struct.* **1999**, *13*, 1069–1095. [[CrossRef](#)]

28. Chen, Y.Z.; Kopp, G.A.; Surry, D. Spatial extrapolation of pressure time series on low buildings using proper orthogonal decomposition. *Wind Struct.* **2004**, *7*, 373–392. [[CrossRef](#)]
29. Li, F.; Ni, Z.; Shen, S. Application of POD to prediction of wind pressure fields of pitched roof. *Eng. Mech.* **2007**, *24*, 68–74.
30. Li, F.; Ni, Z.; Shen, S.; Gu, M. Theory of POD and its application in wind engineering of structures. *J. Vib. Shock.* **2009**, *28*, 29–33. (In Chinese)
31. Li, Y.; Shen, Z. Application of the proper orthogonal decomposition method to wind field reconstruction of models with curved surfaces. *J. Tongji Univ.* **2006**, *34*, 22–26. (In Chinese)
32. Ji, X.; Huang, G.; Zhang, X.; Kopp, G.A. Vulnerability analysis of steel roofing cladding: Influence of wind directionality. *Eng. Struct.* **2018**, *156*, 587–597. [[CrossRef](#)]
33. Cizmas, P.G.; Palacios, A.; O'Brien, T.; Syamlal, M. Proper-orthogonal decomposition of spatio-temporal patterns in fluidized beds. *Chem. Eng. Sci.* **2003**, *58*, 4417–4427. [[CrossRef](#)]
34. Berkooz, G.; Holmes, A.P.; Lumley, J.Y. The proper orthogonal decomposition in the analysis of turbulent flows. *Annu. Rev. Fluid Mech.* **1993**, *25*, 539–575. [[CrossRef](#)]
35. Rowley, C.W.; Marsden, J.E. Reconstruction equations and the Karhunen-Loève expansion for systems with symmetry. *Phys. D* **2000**, *142*, 1–19. [[CrossRef](#)]
36. Yang, Q.; Chen, B.; Wu, Y.; Tamura, Y. Wind-induced response and equivalent static wind load of long-span roof structures by combined Ritz-proper orthogonal decomposition method. *J. Struct. Eng.* **2013**, *139*, 997–1008. [[CrossRef](#)]
37. Zhao, Z.; Chen, Z.; Wang, X.; Xu, H.; Liu, H. Wind-induced response of large-span structures based on POD-pseudo-excitation method. *Adv. Steel Constr.* **2016**, *12*, 1–16.
38. Roy, K.; Lim, J.B.P.; Yousefi, A.M.; Clifton, G.C.; Mahendran, M. Low fatigue response of crest-fixed cold-formed steel drape curved roof claddings. In Proceedings of the Wei-Wen Yu International Specialty Conference on Cold-Formed Steel Structures 2018: Recent Research and Developments in Cold-Formed Steel Design and Construction, St. Louis, MO, USA, 7–8 November 2018.
39. Su, Y.; Li, M.; Yang, Y.; Mann, J.; Liao, H.; Li, X. Experimental investigation of turbulent fluctuation characteristics observed at a moving point under crossflows. *J. Wind Eng. Ind. Aerody.* **2020**, *197*, 104079. [[CrossRef](#)]
40. Su, Y.; Di, J.; Zuo, T.; Li, S.; Qin, F. Buffeting response evaluation of slender linear structures considering the influence of the aspect ratio on the scale effect. *J. Sound Vib.* **2022**, *530*, 116969. [[CrossRef](#)]
41. Li, S.; Li, M.; Liao, H. The lift on an aerofoil in grid-generated turbulence. *J. Fluid Mech.* **2015**, *771*, 16–35. [[CrossRef](#)]
42. Li, S.; Li, M. Spectral analysis and coherence of aerodynamic lift on rectangular cylinders in turbulent flow. *J. Fluid Mech.* **2017**, *830*, 408–438. [[CrossRef](#)]
43. Li, M.; Yang, Y.; Li, M.; Liao, H. Direct measurement of the Sears function in turbulent flow. *J. Fluid Mech.* **2018**, *847*, 768–785. [[CrossRef](#)]
44. Ministry of Housing and Urban-Rural Development of the People's Republic of China. *Load Code for the Design of Building Structures GB 50009-2012*; China Building Industry Press: Beijing, China, 2012. (In Chinese)